Performance Analysis of Wireless Networks With Directional Antennas

Ping-Cheng Yeh, *Member, IEEE*, Wayne E. Stark, *Fellow, IEEE*, and Salam A. Zummo, *Member, IEEE*

***Abstract*—In this paper, we consider wireless networks with directional antennas using slotted ALOHA medium access control. The channel model incorporates the effects of propagation loss and shadowing with Rayleigh fading. By deriving the cumulative distribution function of the signal-to-interference-and-noise ratio (SINR) of a certain link in the network, the outage probability of the link is analyzed. In particular, the analysis works for the arbitrary beam patterns of the directional antennas used in the networks. Moreover, we propose a new parameter, i.e., the array interference factor, which can characterize the average performance of an arbitrary beam pattern in random wireless networks. This provides an efficient way for designers to evaluate the system performance under different beam patterns. The network throughput and the transport capacity of a random wireless network with directional antennas are also analyzed. It is shown that the network transport capacity is of the same order as the square root of the node density, which conforms with the well-known capacity of wireless networks. The analysis is useful for designers to optimize the system performance of wireless networks with directional antennas.**

***Index Terms*—Beam pattern, directional antenna, outage probability, path loss, Rayleigh fading, shadowing, throughput, transport capacity.**

I. Introduction

In a wireless network, when a node transmits a signal to another node, it causes interference to the other nodes in the same network. This limits the number of simultaneous transmissions in a wireless network. Many systems use omnidirectional antennas to avoid having to know the location of the receiver. An omnidirectional antenna transmits a signal to all directions with the same power. Not only does this cause interference to the other nodes, but the power is also wasted in the directions away from the receiving node. The interference limits the number of users that a system can accommodate. This gives rise to the promising idea of using directional antennas in wireless networks.

By using directional antennas, both transmitting and receiving nodes have the ability to generate beam patterns with high transmission gain and reception gain in the direction of each other and low gain elsewhere. The enhanced power efficiency enables the extension of the battery life of a node, which is crucial for wireless communication devices. Furthermore, the interference problem is significantly reduced, because only nodes with receiving antennas pointing at the main beam of a transmitting node are severely interfered by the transmitting node. This allows the system to have a larger number of users than with omnidirectional antennas. As a result, directional antenna technology is widely considered for wireless networks, such as IEEE 802.11 [1], [2], IEEE 802.16 [3], and IEEE 802.15.3c [4].

To get the best system performance out of such wireless networks, system designers need to know the relation between the network performance and the system parameters. In the literature, only a few efforts have attempted to analyze the performance of wireless networks with directional antennas. In [5] and [6], the outage probability of wireless networks with omnidirectional antennas has been analyzed. The outage probability of wireless networks using switched beam antennas has been analyzed in [7]. However, the antenna radiation diagram used in this paper is very simple. The result cannot be applied to analyze system performance when a realistic beam pattern is considered. In [8], the outage probability of a receiver using a smart antenna with a fixed number of interferers under Rayleigh and Rician fading has been analyzed. The medium access control (MAC) protocol is assumed to be slotted ALOHA [9] in [6] and [7], but it is unspecified in [5] and [8]. None of past research efforts considered the performance of a wireless network using an arbitrary antenna beam pattern and the effect of specific coding and modulation schemes on system performance.

In this paper, we derive the outage probability of wireless networks using an arbitrary beam pattern under a realistic channel model, which includes the effects of path loss, shadowing, and Rayleigh fading. Slotted ALOHA [9] is used for the MAC protocol. By combining with performance analysis of bit-interleaved coded modulation (BICM) and turbo codes in [10] and [11], we can evaluate the performance of a wireless network with specific coding and modulation used in the physical layer. One thing worth noting is that we find that the system performance and the beam pattern used are related through a characteristic value of the beam pattern, which we call the *array interference factor* (AIF). The AIF can very easily be computed for any radiation diagram, which provides an efficient way for

Manuscript received January 23, 2006; revised January 5, 2007, August 4, 2007, and August 20, 2007. This paper was presented in part at the IEEE Proceedings of the Military Communications Conference, Monterey, CA, October 2004. This work was supported in part by National Taiwan University, in part by the R.O.C. National Science Council under Grant NSC-95-2221-E-002-001, and in part by King Fahd University of Petroleum and Minerals under Grant FT040009. The review of this paper was coordinated by Dr. L. Cai.

P.-C. Yeh is with the Department of Electrical Engineering and the Graduate Institute of Communication Engineering, National Taiwan University, Taipei 10617, Taiwan, R.O.C. (e-mail: pcyeh@ntu.edu.tw).

W. E. Stark is with the Department of Electrical Engineering and Computer Science, University of Michigan, Ann Arbor, MI 48109 USA (e-mail: stark@eecs.umich.edu).

S. A. Zummo is with the Department of Electrical Engineering, King Fahd University of Petroleum and Minerals, Dhahran 31261, Saudi Arabia (e-mail: zummo@kfupm.edu.sa).

Color versions of one or more of the figures in this paper are available online at http://ieeexplore.ieee.org.

Digital Object Identifier 10.1109/TVT.2008.917223

the performance comparison of different beam patterns; the one with smaller AIF generally has better performance than the others.

Initially, we assume that the transmitting and receiving nodes know the exact direction of each other in the outage probability derivation. However, this is not usually true in reality due to the MAC protocol or the accuracy of the direction estimation algorithm used. For instance, in the MAC protocols proposed for IEEE 802.11 with directional antennas [1], [2], the nodes are designed with a finite number of beam directions. Hence, the transmitting and receiving nodes are not always perfectly aligned. The direction estimation error affects the system performance, and generally, directional antennas of smaller beam widths suffer more from the problem. Without further analyzing the effect of this direction estimation error on network performance, one cannot make a fair performance comparison of different beam patterns since patterns of smaller beam widths always have better performance if there exists no direction estimation error. Hence, the outage probability, given the existence of the direction estimation error between the node pair, is further analyzed in this paper.

As mentioned earlier, one major motivation of this paper is optimization of the system performance for wireless networks using directional antennas. Other than the outage probability, common performance measures of wireless networks include network throughput and transport capacity [12]. Both measures are derived in this paper. It is shown that the network transport capacity of a wireless network using directional antennas is of order $\Theta(\sqrt{\lambda_M})$, where λ_M is the node density of the network. Note that $f(n) = \Theta(g(n))$ if $f(n) = O(g(n))$ and $g(n) = O(f(n))$ (Knuth's notation). This finding conforms with the well-known transport capacity of wireless networks derived by Gupta and Kumar in [12].

The remainder of this paper is organized as follows: In Section II, a brief introduction to the system model and the channel model is given. In Section III, we derive the outage probability in a wireless network using a simplified beam pattern, given that the transmitting and receiving nodes are perfectly aligned. The analysis is then generalized to the case of an arbitrary beam pattern. In Section IV, we analyze the outage probability under the effect of direction estimation error between the node pair. In Section V, the network throughput and transport capacity are both derived. Finally, we address the conclusions in Section VI.

II. Model Description

Consider a wireless network as shown in Fig. 1. We are interested in the performance of the communication link between two reference nodes Tx (transmitting node) and Rx (receiving node). We first assume that all nodes use directional antennas for transmission and omnidirectional antennas for reception. Later, we will generalize the analysis to the case where directional antennas are used for both transmission and reception. We assume that all nodes use the same transmitting beam pattern. A typical beam pattern $g(\theta)$ is shown in Fig. 2, where $g(\theta)$ denotes the power gain of the transmitting antenna relative to an omnidirectional antenna in the direction of θ. For

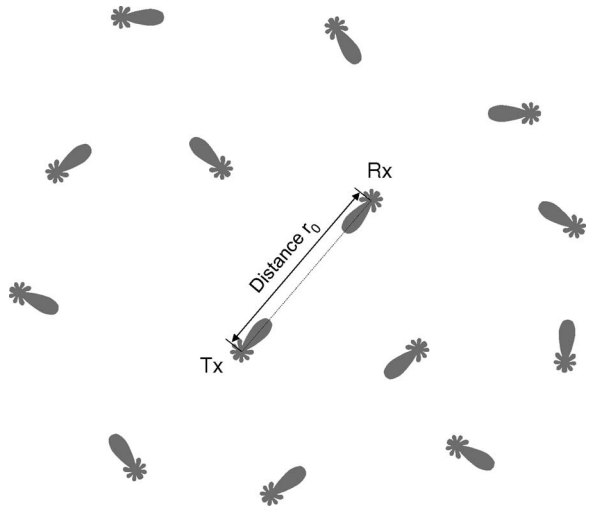

Fig. 1. Wireless network using directional antennas.

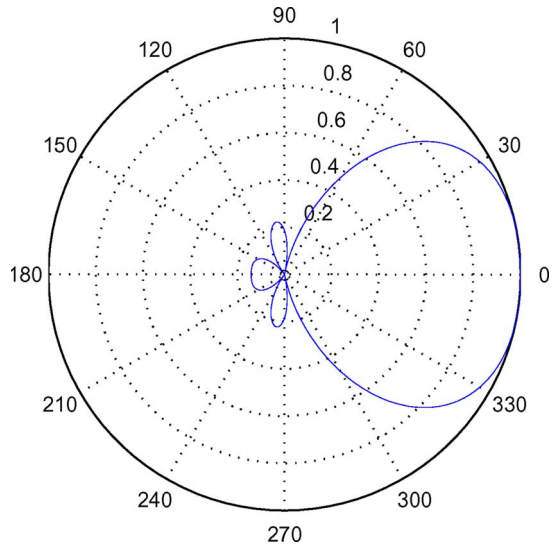

Fig. 2. Beam pattern $g(\theta)$.

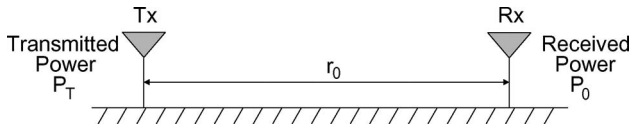

Fig. 3. Channel between Tx and Rx.

an omnidirectional antenna, $g(\theta) = 1$ for all θ. We make no assumption on how the directional antennas are formed: They can be either mechanically steered or electronically formed. The antennas are assumed to be devoid of any mutual correlation. Although the beam pattern considered in this paper is 2-D, the result can be generalized to 3-D beam patterns. Finally, it is assumed that all nodes have perfect knowledge of their own channels.

We use the same channel model as in [5], as shown in Fig. 3. Assume that the distance between Tx and Rx is r_0 and that Rx is in the direction of θ_0 from Tx. When Tx transmits power P_T, the received power at Rx is then $P_0 = P_T g(\theta_0)\ \zeta_0\ \xi_0^2$, where ζ_0 accounts for path loss and shadowing effect. It is assumed that ζ_0 is constant for, at least, a packet duration T and that

it is lognormal distributed with conditional probability density function (pdf), i.e.,

$$f(\zeta_0 \mid r_0) = \frac{1}{\sqrt{2\pi}\sigma\rho\zeta_0}\, e^{-\frac{1}{2}\frac{\left(\log_e \zeta_0 - \log_e\left(Kr_0^{-\eta}\right)\right)^2}{\sigma^2\rho^2}} \tag{1}$$

where ρ denotes the constant $\log_e 10/10$, and $Kr_0^{-\eta}$ is the average attenuation level due to path loss. The constant K denotes the average attenuation level measured at a reference distance from the transmitting node, and η is the path loss exponent, which ranges from 2.0 to 6.0, depending on the type of channel [13]. In an urban area, η is in the range of about 2.7–3.5. In an obstructed environment or in buildings, where signals suffer more from path loss, η is in the range of about 4.0–6.0. In addition, note that σ is usually denoted in decibels. Typical values for σ are in the range of 5–10 dB.

Fading level ξ_0 is a random variable that accounts for the Rayleigh fading. If ξ_0 is Rayleigh distributed, then ξ_0^2 is exponentially distributed [14]. Hence, the conditional pdf of P_0, given ζ_0, is

$$f_0(P_0 \mid \zeta_0) = \frac{1}{P_T g(\theta_0)\zeta_0}\, e^{-\frac{P_0}{P_T g(\theta_0)\zeta_0}} \tag{2}$$

and the conditional cumulative density function (cdf) is

$$F_0(P_0 \mid \zeta_0) = 1 - e^{-\frac{P_0}{P_T g(\theta_0)\zeta_0}}. \tag{3}$$

The channel between any interfering node and Rx follows the previously described model, except that the distance can be different. In addition, the signal from each interfering node to Rx is independently shadowed and independently Rayleigh faded. We also assume that the signal power from an interfering node is constant throughout each packet duration.

The nodes are assumed to be randomly distributed on the 2-D plane as a Poisson point process. Let λ_M denote the average node density. For any disc of radius r on the plane, the number of nodes N_r in the disc has a Poisson distribution $\text{POI}(\lambda_M \pi r^2)$, i.e., $\Pr\{N_r = k\} = e^{-\lambda_M \pi r^2}(\lambda_M \pi r^2)^k/k!$. The MAC protocol is assumed to be slotted ALOHA. All nodes are synchronized, and every packet is transmitted at the beginning of the time slot, right after the packet is generated. Each time slot is of duration T, which is the same as the packet duration. The nodes in the ALOHA ad hoc network are not allowed to simultaneously transmit and receive, i.e., the nodes in transmitting mode cannot be in receiving mode at the same time and *vice versa*. Each node generates data packets, which are modeled by a Bernoulli process of rate p, i.e., the packets are generated with probability p in each slot. Hence, given that there are N_r nodes in the network (excluding Tx and Rx), the number of nodes that actually interfere with Rx is binomially distributed as $\text{BIN}(N_r, p)$.

III. Outage Probability Analysis

In this section, we analyze the performance of the link between Tx and Rx by deriving the outage probability of the link under slow fading. By slow fading, we mean that the fading level of the target link between Tx and Rx is constant for at least one packet duration. This is usually the case when Tx, Rx, and the environment are all of low mobility. We first derive the outage probability for a simplified beam pattern of Tx, as shown in Fig. 4, in Section III-A. Then, the analysis is generalized for any arbitrary shape of beam patterns used by Tx and Rx in Section III-B, and several numerical examples are shown in Section III-C. In this part of the analysis, we assume that Tx is always perfectly aligned to Rx, i.e., $\theta = 0$ always points to the direction of Rx. Imperfect alignment case is later analyzed in Section IV.

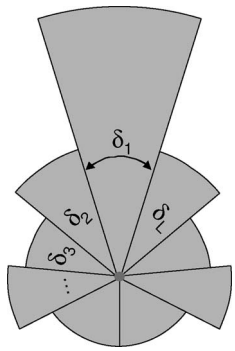

Fig. 4. Simplified beam pattern.

A. Simplified Beam Pattern

First, consider the simplified beam pattern shown in Fig. 4. The beam pattern has L beams. Beam i, $i = 1, 2, \ldots, L$ has angular beam width δ_i (in radians) and gain g_i with respect to the omnidirectional antenna of the same transmitting power. Without loss of generality, beam 1 is always the beam with the largest gain and is always pointing at Rx. The outage probability of the link between Tx and Rx is defined by

$$\phi_{L,r_0}(b) = P\{\text{Outage}\} \triangleq P\left\{\frac{P_0}{P_I + N} < b\right\} \tag{4}$$

where P_0 is the received power, P_I is the interference power, and N is the noise power at Rx. If we denote the energy per symbol received at Rx (from Tx) by E_s and the symbol duration by T_s, it is easy to see that $P_0 = E_s/T_s$ and $N = N_0/T_s$, where N_0 denotes the noise power spectral density. It is assumed that the outage occurs whenever the signal-to-interference-and-noise ratio (SINR) at Rx is less than a certain threshold b, which causes the failure of the channel coding and modulation to maintain the small packet error rate (PER) required by the data transmission. Hence, the SINR threshold b depends on the coding and modulation used by Tx. In a slow-faded channel, the SINR should remain constant during the whole packet duration. When we determine the value of b for a specific coding and modulation scheme, we should refer to the performance of the coding and modulation scheme in an additive white Gaussian noise (AWGN) channel. The analyses in [10] and [11] enable us to plot the PER versus signal-to-noise ratio (SNR) for various coded modulation schemes and turbo codes over AWGN and different fading channels. If we model the interference as noise, we can easily determine the value of b from the PER analysis.

The key concept of computing $\phi_{L,r_0}(b)$ is to compute $\phi_{L,r_0}(b,a) = P\{(P_0/(P_I(a) + N)) < b\}$ first, where $P_I(a)$ is defined as the total interference power from interferers

TABLE I
SUMMARY OF THE DEFINED SYMBOLS

Symbol	Meaning
λ_M	Node density of the wireless network.
b	SINR threshold for the coding/modulation to achieve the required PER.
η	Path loss exponent.
σ	Standard deviation of the log-normal shadowing.
ρ	Scaling constant $\frac{\log_e 10}{10}$.
$g(\theta)$	Power gain of the directional antenna in the direction of θ.
g_i	Power gain of beam i of the simplified beam pattern in Fig. 4.
δ_i	Beam width of beam i of the simplified beam pattern.
θ_0	Direction of Rx from Tx.
P_T	Transmitted signal power at Tx.
r_0	Distance from Tx to Rx.
ζ_0	Path loss and shadowing at Rx experienced by the signal from Tx.
ξ_0	Power variation from Rayleigh fading between Tx and Rx.
P_0	Received signal Power at Rx from Tx.
K_i	Number of nodes in group i, i.e., the group of nodes (Tx excluded) within a disc of radius a centered at Rx that point at Rx with beam i, $i = 1, \cdots, L$.
$\boldsymbol{K_a}$	$\boldsymbol{K_a} = (K_1, K_2, \cdots, K_L)$.
I_i	Number of active nodes among the K_i nodes in group i that are actually interfering Rx, $i = 1, \cdots, L$.
$\boldsymbol{I_a}$	$\boldsymbol{I_a} = (I_1, I_2, \cdots, I_L)$.
$r_{i,j}$	Distance from interferer j in group i to Rx, $i = 1, \cdots, L$, $j = 1, \cdots, I_i$.
$\boldsymbol{r_i}$	$\boldsymbol{r_i} = (r_{i,1}, r_{i,2}, \cdots, r_{i,I_i})$, $i = 1, \cdots, L$.
$\boldsymbol{r_a}$	$\boldsymbol{r_a} = [\boldsymbol{r_1}, \boldsymbol{r_2}, \cdots, \boldsymbol{r_L}]$.
$\zeta_{i,j}$	Path loss and shadowing at Rx experienced by the interference from interferer j in group i , $i = 1, \cdots, L$ $j = 1, \cdots, I_i$.
$\boldsymbol{\zeta_i}$	$\boldsymbol{\zeta_i} = (\zeta_{i,1}, \zeta_{i,2}, \cdots, \zeta_{i,I_i})$, $i = 1, \cdots, L$.
$\boldsymbol{\zeta_a}$	$\boldsymbol{\zeta_a} = [\boldsymbol{\zeta_1}, \boldsymbol{\zeta_2}, \cdots, \boldsymbol{\zeta_L}]$.
$P_{i,j}$	Received interference power at Rx from interferer j in group i, $i = 1, \cdots, L$, $j = 1, \cdots, I_i$.
$\boldsymbol{P_i}$	$\boldsymbol{P_i} = (P_{i,1}, P_{i,2}, \cdots, P_{i,I_i})$, $i = 1, \cdots, L$.
$\boldsymbol{P_a}$	$\boldsymbol{P_a} = [\boldsymbol{P_1}, \boldsymbol{P_2}, \cdots, \boldsymbol{P_L}]$.

located within a distance a from Rx. After taking the limit as a goes to infinity, we can obtain the outage probability $\phi_{L,r_0}(b) = \lim_{a\to\infty} \phi_{L,r_0}(b,a)$. Consider the nodes in the disc of radius a centered at Rx (Tx excluded). We classify them into L groups. The nodes in the ith group all point at Rx with their beam i. Let $\boldsymbol{K_a} \triangleq (K_1, K_2, \ldots, K_L)$ denote the number of nodes in each group. The number of nodes in a disc of radius a has a Poisson distribution POI($\lambda_M \pi a^2$). If we assume that the direction of any node to its receiving node is uniformly distributed between 0 and 2π, then the probability of a node pointing at Rx with beam i is $\delta_i/2\pi$, which is proportional to the angular beam width δ_i. This implies that K_i has a Poisson distribution POI($\lambda_M a^2 \delta_i/2$). Since the K_i's are independent

$$P(\boldsymbol{K_a}) = \prod_{i=1}^{L} \frac{e^{\frac{-\lambda_M a^2 \delta_i}{2}} \left(\frac{\lambda_M a^2 \delta_i}{2}\right)^{K_i}}{K_i!}. \tag{5}$$

Among the K_i nodes in the ith group, the number of nodes that actually transmit packets and thus interfere with Rx, i.e., I_i, is of distribution BIN(K_i, p). Define $\boldsymbol{I_a} \triangleq (I_1, I_2, \ldots, I_L)$. Then

$$P(\boldsymbol{I_a} \mid \boldsymbol{K_a}) = \prod_{i=1}^{L} \binom{K_i}{I_i} p^{I_i} (1-p)^{K_i - I_i}. \tag{6}$$

To analyze the outage probability, number those I_i interferers in the ith group from 1 to I_i. The distance from interferer j in group i to Rx is denoted by $r_{i,j}$. The pdf of $r_{i,j}$, given that the interferer is in the disc of radius a centered at Rx, is of the form

$$f_a(r_{i,j}) = \frac{2\pi r_{i,j}}{\pi a^2} = \frac{2 r_{i,j}}{a^2}. \tag{7}$$

For later use, we define vector $\boldsymbol{r_a} \triangleq [\boldsymbol{r_1}, \boldsymbol{r_2}, \ldots, \boldsymbol{r_L}]$, where $\boldsymbol{r_i} = (r_{i,1}, r_{i,2}, \ldots, r_{i,I_i})$, $i = 1, 2, \ldots, L$.

The path loss and shadowing at Rx experienced by the interference from interferer j in group i is denoted by $\zeta_{i,j}$. From (1), we have

$$f(\zeta_{i,j} \mid r_{i,j}) = \frac{1}{\sqrt{2\pi}\sigma\rho\zeta_{i,j}} e^{-\frac{1}{2}\frac{\left(\log_e \zeta_{i,j} - \log_e\left(K r_{i,j}^{-\eta}\right)\right)^2}{\sigma^2\rho^2}}. \tag{8}$$

Define vector $\boldsymbol{\zeta_a} \triangleq [\boldsymbol{\zeta_1}, \boldsymbol{\zeta_2}, \ldots, \boldsymbol{\zeta_L}]$, where $\boldsymbol{\zeta_i} = (\zeta_{i,1}, \zeta_{i,2}, \ldots, \zeta_{i,I_i})$, $i = 1, 2, \ldots, L$.

The received interference power at Rx from interferer j in group i is denoted by $P_{i,j}$. The conditional distribution of $P_{i,j}$, given $\zeta_{i,j}$, is exponentially distributed, as described in Section II. The conditional pdf is

$$f(P_{i,j} \mid \zeta_{i,j}) = \frac{1}{P_T g_i \zeta_{i,j}} e^{-\frac{P_{i,j}}{P_T g_i \zeta_{i,j}}}. \tag{9}$$

Define vector $\boldsymbol{P_a} \triangleq [\boldsymbol{P_1}, \boldsymbol{P_2}, \ldots, \boldsymbol{P_L}]$, where $\boldsymbol{P_i} = (P_{i,1}, P_{i,2}, \ldots, P_{i,I_i})$, $i = 1, 2, \ldots, L$.

Finally, recall that r_0, ζ_0, and P_0 are the distance, path loss, and received power at Rx from Tx, respectively. Since Tx is pointing at Rx with beam 1, which has a gain of g_1, the cdf of P_0, given ζ_0, in (3) becomes

$$F_0(P_0 \mid \zeta_0) = 1 - e^{-\frac{P_0}{P_T g_1 \zeta_0}}. \tag{10}$$

Due to the large number of symbols defined for the later analysis, a summary of all defined symbols is given in Table I. Before deriving the outage probability, we first give a high-level description about our derivation process. Probability

$P\{(P_0/(P_I(a)+N)) < b\}$ is determined by b, a, and the realization of a random vector $\mathbf{x} \triangleq (\boldsymbol{K_a}, \boldsymbol{I_a}, \boldsymbol{r_a}, \boldsymbol{\zeta_a}, \boldsymbol{P_a}, r_0, \zeta_0, P_0)$. If we denote the pdf of $\mathbf{x}$ by $f(\mathbf{x})$, then $\phi_{L,r_0}(b,a) = P\{(P_0/(P_I(a)+N)) < b\}$ is simply

$$\phi_{L,r_0}(b,a) = \int_S f(x)dx$$

where $S = \{\mathbf{x} : (P_0/(P_I(a)+N)) < b\}$. The order of integration (with respect to the elements of $\mathbf{x}$) that we take is P_0, $\boldsymbol{P_a}$, $\boldsymbol{r_a}$, $\boldsymbol{\zeta_a}$, $\boldsymbol{I_a}$, $\boldsymbol{K_a}$, and, finally, ζ_0. By first taking the integration with respect to P_0 and $\boldsymbol{P_a} = \{P_{i,j}\}$, we can obtain the conditional outage probability, given $\boldsymbol{K_a}$, $\boldsymbol{I_a}$, $\boldsymbol{r_a}$, $\boldsymbol{\zeta_a}$, r_0, and ζ_0. It can easily be done by first applying the cdf of P_0 in (10) and then integrating with respect to the exponential pdf of the independently distributed $P_{i,j}$ in (9). This results in

$$\begin{aligned}
&\phi_{L,r_0}(b,a \mid \boldsymbol{K_a}, \boldsymbol{I_a}, \boldsymbol{r_a}, \boldsymbol{\zeta_a}, \zeta_0) \\
&\quad = P\{P_0 < bP_I(a) + bN \mid \boldsymbol{K_a}, \boldsymbol{I_a}, \boldsymbol{r_a}, \boldsymbol{\zeta_a}, \zeta_0\} \\
&\quad = \int_0^\infty \cdots \int_0^\infty F_0\left(b\sum_{i=1}^{L}\sum_{j=1}^{I_i} P_{i,j} + bN\right) \\
&\qquad \times \prod_{i=1}^{L}\prod_{j=1}^{I_i} [f(P_{i,j} \mid \zeta_{i,j})\, dP_{i,j}] \\
&\quad = 1 - e^{-\frac{bN}{P_T g_1 \zeta_0}} \prod_{i=1}^{L}\prod_{j=1}^{I_i}\left[\frac{1}{1+\frac{bg_i\zeta_{i,j}}{g_1\zeta_0}}\right]. \qquad (11)
\end{aligned}$$

Next, we take the expectation with respect to $\boldsymbol{r_a}$ and $\boldsymbol{\zeta_a}$ and substitute y for $(\log_e \zeta_{i,j} - \log_e(Kr_{i,j}^{-\eta}))$ and x for $(\log_e \zeta_0 - \log_e(Kr_0^{-\eta}))$. We can thus obtain (12), shown at the bottom of the page, where

$$I_a(x,\psi) \triangleq \frac{1}{\sqrt{2\pi}\sigma\rho a^2}\int_{-\infty}^{\infty} e^{-\frac{y^2}{2\sigma^2\rho^2}}dy \int_0^a \frac{2rdr}{1+\psi b e^{y-x}\left(\frac{r_0}{r}\right)^\eta}. \qquad (13)$$

Next, by taking the expectation of (12) with respect to the lognormal pdf of ζ_0 in (1), we have

$$\begin{aligned}
\phi_{L,r_0}(b,a \mid \boldsymbol{K_a}, \boldsymbol{I_a}) &= 1 - \int_0^\infty e^{-\frac{bN}{P_T g_1 \zeta_0}} \prod_{i=1}^{L}\left[I_a\left(x, \frac{g_i}{g_1}\right)\right]^{I_i} \\
&\quad \times \frac{1}{\sqrt{2\pi}\sigma\rho\zeta_0} e^{-\frac{1}{2}\frac{\left(\log_e\zeta_0 - \log_e\left(Kr_0^{-\eta}\right)\right)^2}{\sigma^2\rho^2}} d\zeta_0 \\
&= 1 - \frac{1}{\sqrt{2\pi}\sigma\rho}\int_{-\infty}^{\infty} e^{-\frac{be^{-x}}{\gamma_c} - \frac{x^2}{2\sigma^2\rho^2}} \\
&\quad \times \prod_{i=1}^{L}\left[I_a\left(x, \frac{g_i}{g_1}\right)\right]^{I_i} dx \qquad (14)
\end{aligned}$$

where $\gamma_c = P_T K g_1 / N r_0^\eta$ is the average received SNR at Rx from Tx, and recall that x is again used to substitute for $(\log_e \zeta_0 - \log_e(Kr_0^{-\eta}))$. Now, taking the expectation with respect to $\boldsymbol{K_a}$ and $\boldsymbol{I_a}$, we have the following expression:

$$\begin{aligned}
&\phi_{L,r_0}(b,a) \\
&\quad = \sum_{K_1,\ldots,K_L} P(\boldsymbol{K_a}) \sum_{I_1,\ldots,I_L} \phi_{L,r_0}(b,a|\boldsymbol{K_a}, \boldsymbol{I_a}) P(\boldsymbol{I_a}|\boldsymbol{K_a}) \\
&\quad = 1 - \sum_{K_1,\ldots,K_L}\prod_{i=1}^{L}\left[\frac{e^{\frac{-\lambda_M a^2\delta_i}{2}}\left(\frac{\lambda_M a^2\delta_i}{2}\right)^{K_i}}{K_i!}\right] \\
&\qquad \times \frac{1}{\sqrt{2\pi}\sigma\rho}\int_{-\infty}^{\infty} e^{-\frac{be^{-x}}{\gamma_c} - \frac{x^2}{2\sigma^2\rho^2}} \\
&\qquad \times \prod_{i=1}^{L}\left[1 + p\left(I_a\left(x, \frac{g_i}{g_1}\right) - 1\right)\right]^{K_i} dx \\
&\quad = 1 - \frac{1}{\sqrt{2\pi}\sigma\rho}\int_{-\infty}^{\infty} \exp\left\{\sum_{i=1}^{L}\frac{\lambda_M a^2\delta_i p}{2} \times \left[I_a\left(x, \frac{g_i}{g_1}\right) - 1\right]\right. \\
&\qquad \left. - \frac{be^{-x}}{\gamma_c} - \frac{x^2}{2\sigma^2\rho^2}\right\} dx. \qquad (15)
\end{aligned}$$

$$\begin{aligned}
\phi_{L,r_0}(b,a \mid \boldsymbol{K_a}, \boldsymbol{I_a}, \zeta_0) &= \int_0^\infty \cdots \int_0^\infty \phi_{L,r_0}(b,a \mid \boldsymbol{K_a}, \boldsymbol{I_a}, \boldsymbol{r_a}, \boldsymbol{\zeta_a}, \zeta_0) \prod_{i=1}^{L}\prod_{j=1}^{I_i} [f(\zeta_{i,j} \mid r_{i,j}) f_a(r_{i,j}) dr_{i,j} d\zeta_{i,j}] \\
&= 1 - e^{-\frac{bN}{P_T g_1 \zeta_0}} \prod_{i=1}^{L}\prod_{j=1}^{I_i}\left[\int_0^a \frac{2r_{i,j}dr_{i,j}}{a^2}\int_0^\infty \frac{e^{-\frac{1}{2}\frac{\left(\log_e\zeta_{i,j} - \log_e\left(Kr_{i,j}^{-\eta}\right)\right)^2}{\sigma^2\rho^2}} d\zeta_{i,j}}{\left(1+\frac{bg_i\zeta_{i,j}}{g_1\zeta_0}\right)\left(\sqrt{2\pi}\sigma\rho\zeta_{i,j}\right)}\right] \\
&= 1 - e^{-\frac{bN}{P_T g_1 \zeta_0}} \prod_{i=1}^{L}\prod_{j=1}^{I_i}\left[\frac{1}{\sqrt{2\pi}\sigma\rho}\int_0^a \frac{2r_{i,j}dr_{i,j}}{a^2}\int_{-\infty}^{\infty} \frac{e^{-\frac{y^2}{2\sigma^2\rho^2}}dy}{1+\frac{g_i b}{g_1}e^{y-x}\left(\frac{r_0}{r_{i,j}}\right)^\eta}\right] \\
&= 1 - e^{-\frac{bN}{P_T g_1 \zeta_0}} \prod_{i=1}^{L}\prod_{j=1}^{I_i}\left[\frac{1}{\sqrt{2\pi}\sigma\rho a^2}\int_{-\infty}^{\infty} e^{-\frac{y^2}{2\sigma^2\rho^2}}dy \int_0^a \frac{2r_{i,j}dr_{i,j}}{1+\frac{g_i b}{g_1}e^{y-x}\left(\frac{r_0}{r_{i,j}}\right)^\eta}\right] \\
&= 1 - e^{-\frac{bN}{P_T g_1 \zeta_0}} \prod_{i=1}^{L}\left[I_a\left(x, \frac{g_i}{g_1}\right)\right]^{I_i} \qquad (12)
\end{aligned}$$

Note that the last line of (15) is obtained by first moving the summation part into the integral and then applying the moment-generating function formula of Poisson distribution (recall that the K_i's are independent Poisson random variables).

To get the outage probability, we need to take the limit of (15) as a goes to ∞. The limit of $a^2(I_a(x,\psi)-1)$ as a goes to ∞ is derived in [5] as

$$\lim_{a\to\infty} a^2\left(I_a(x,\psi)-1\right) = -r_0^2 e^{\frac{2\sigma^2\rho^2}{\eta^2}} \frac{2\pi}{\eta}\csc\left(\frac{2\pi}{\eta}\right) b^{\frac{2}{\eta}} \psi^{\frac{2}{\eta}} e^{\frac{-2x}{\eta}}. \tag{16}$$

After some simplifications from (15), we can obtain the final form of the outage probability

$$\phi_{L,r_0}(b) = 1 - \frac{1}{\sqrt{2\pi}\sigma\rho}\int_{-\infty}^{\infty} \exp\left\{-\Lambda(b,x) r_0^2 \left[\sum_{i=1}^{L} \frac{\delta_i}{2\pi}\left(\frac{g_i}{g_1}\right)^{\frac{2}{\eta}}\right] - \frac{be^{-x}}{\gamma_c} - \frac{x^2}{2\sigma^2\rho^2}\right\} dx \tag{17}$$

where

$$\Lambda(b,x) \triangleq \lambda_M \pi p e^{\frac{2\sigma^2\rho^2}{\eta^2}} \frac{2\pi}{\eta}\csc\left(\frac{2\pi}{\eta}\right) b^{\frac{2}{\eta}} e^{\frac{-2x}{\eta}}. \tag{18}$$

Although $\phi_{L,r_0}(b)$ is not in closed form, the integral can easily be computed through numerical integration.

B. Arbitrary Beam Pattern and AIF

Now, consider a more realistic beam pattern such as the one in Fig. 2. Note that Fig. 4 will converge to Fig. 2 as L goes to ∞ and δ_i goes to 0. Taking the limit of (17), we have the outage probability $\phi_{r_0}(b)$ of the realistic beam pattern

$$\begin{aligned}\phi_{r_0}(b) &= \lim_{\substack{L\to\infty \\ \delta_i\to 0}} \phi_{L,r_0}(b) \\ &= 1 - \frac{1}{\sqrt{2\pi}\sigma\rho}\int_{-\infty}^{\infty} \exp\left\{-\Lambda(b,x) r_0^2 \left[\frac{1}{2\pi}\int_0^{2\pi}\left(\frac{g(\theta)}{g(\theta_0)}\right)^{\frac{2}{\eta}} d\theta\right] - \frac{be^{-x}}{\gamma_c} - \frac{x^2}{2\sigma^2\rho^2}\right\} dx.\end{aligned} \tag{19}$$

Notice that $\phi_{r_0}(b)$ depends on the beam pattern only through $(1/2\pi)\int_0^{2\pi}(g(\theta)/g(\theta_0))^{2/\eta}d\theta$. Hence, we propose a new parameter, i.e., the AIF, for any beam pattern

$$\mathcal{A} \triangleq \frac{1}{2\pi}\int_0^{2\pi}\left(\frac{g(\theta)}{g(\theta_0)}\right)^{\frac{2}{\eta}} d\theta \tag{20}$$

which fully characterizes the performance of the beam pattern in random networks. For an omnidirectional antenna, $\mathcal{A}=1$. It is easy to see that, when $\mathcal{A}$ becomes large, the integrand of (19) becomes small, and thus, $\phi_{r_0}(b)$ becomes large. Hence, $\phi_{r_0}(b)$ is a monotonic increasing function of AIF $\mathcal{A}$. This is due to the fact that any beam pattern with smaller AIF value will create (receive) less interference to (from) the system and thus have a better performance. With the introduction of AIF, now, we can compare the performance of different beam patterns by simply comparing the AIF of each beam pattern.

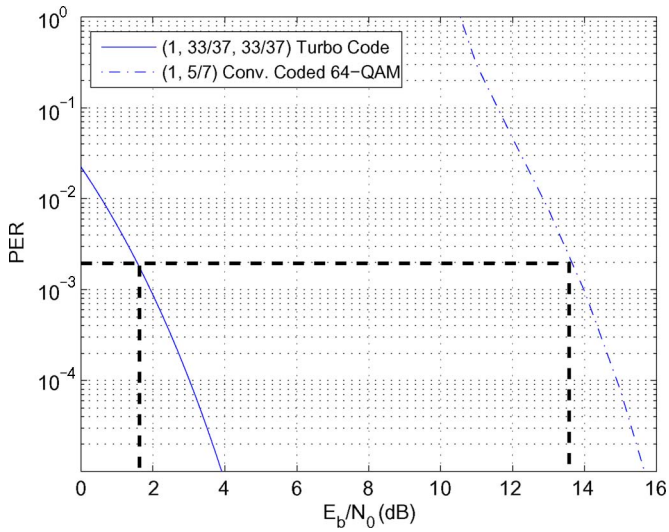

Fig. 5. PER union bounds of (1, 33/37, 33/37) turbo code and bit-interleaved (1, 5/7) convolutional-coded 64-QAM in AWGN channel.

For systems that use directional antennas for both transmission and reception, the outage probability is a little more complicated. Recall that, in the previous analysis, the interferers are classified into L groups according to the beam (in Fig. 4) with which they point at the omnidirectional node Rx. This results in the L-term summation in (17) and, later, the AIF in (19). If Rx now uses the directional antenna with the simplified beam pattern in Fig. 4, then we have to classify the interferers into L^2 groups, depending on the beam of an interferer and the beam of Rx with which they point at each other. As a result, the summation of L terms in (17) becomes a summation of L^2 terms, which can further be factorized into a product of two L-term summations. The result can then be generalized for the case of arbitrary receiving beam patterns as

$$\phi_{r_0}(b) = 1 - \frac{1}{\sqrt{2\pi}\sigma\rho} \times \int_{-\infty}^{\infty} \exp\left\{-\Lambda(b,x) r_0^2 \mathcal{A}_t\mathcal{A}_r - \frac{be^{-x}}{\gamma_c} - \frac{x^2}{2\sigma^2\rho^2}\right\} dx \tag{21}$$

where $\mathcal{A}_t$ and $\mathcal{A}_r$ are the AIF values of the transmitting and receiving beam patterns, respectively.

C. Numerical Examples

In this section, we use the outage probability analysis to evaluate the performance of the wireless networks using different coded modulation schemes. Two different coded modulation schemes are considered: BICM (bit-interleaved rate-1/2 (1, 5/7) convolutional-coded 64-state quadrature amplitude modulation (64-QAM), coded packet length = interleaver size = 2052 bits) and rate-1/3 (1, 33/37, 33/37) turbo code (coded packet length = 2052 bits) with binary phase-shift keying. As mentioned earlier, the value of threshold b is determined by the performance of the coded modulation used in the AWGN channel. By applying the performance analyses in [10] and [11], we can obtain tight bounds on the PER of BICM and turbo code in the AWGN channel, as shown in Fig. 5. If one

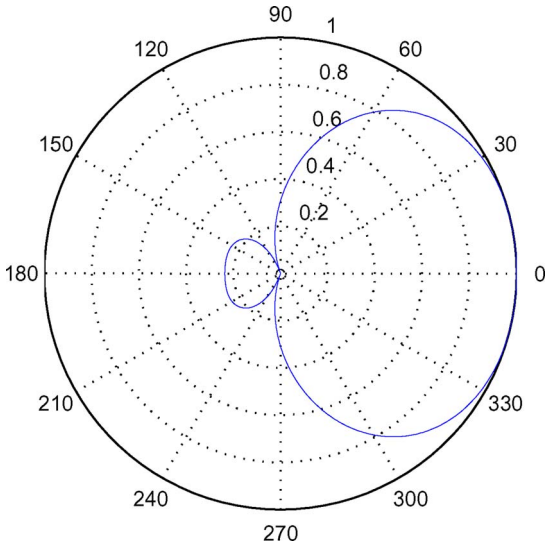

Fig. 6. Beam pattern 1 (generated by six antenna elements with an AIF of 0.6569 at $\eta = 4$ and 0.5699 at $\eta = 2.7$).

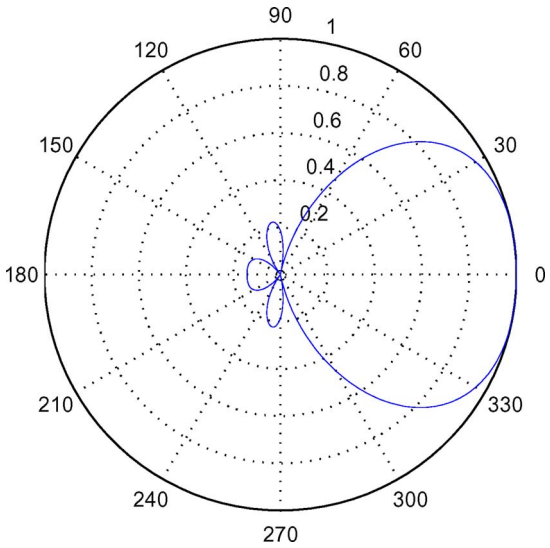

Fig. 7. Beam pattern 2 (generated by ten antenna elements with an AIF of 0.5511 at $\eta = 4$ and 0.4545 at $\eta = 2.7$).

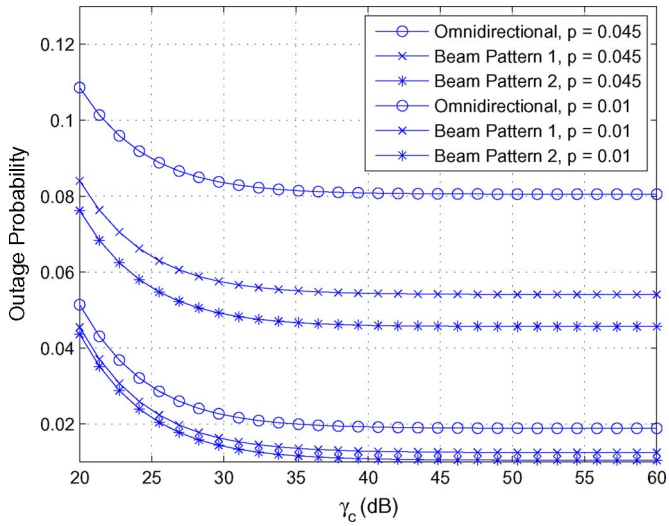

Fig. 8. Outage probability versus average received SNR γ_c with (1, 33/37, 33/37) turbo code in an obstructed environment, $\lambda_M = 20.0$ node/km^2, $b = 1.6$ dB, $\sigma = 6$ dB, $\eta = 4$, and $r_0 = 0.1$ km.

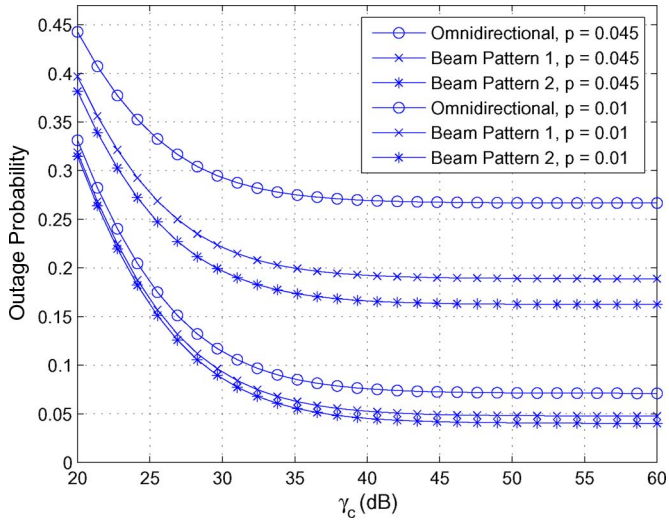

Fig. 9. Outage probability versus average received SNR γ_c with (1, 5/7) convolutional-coded 64-QAM in an obstructed environment, $\lambda_M = 20.0$ node/km^2, $b = 13.5$ dB, $\sigma = 6$ dB, $\eta = 4$, and $r_0 = 0.1$ km.

packet error out of every 500 packet transmissions, i.e., a PER of 2×10^{-3}, is considered to be the threshold of acceptable communication quality, then, from the figure, we can see that threshold b should be 1.6 dB for the turbo-coded system and 13.5 dB for BICM. The BICM system has a nine times higher bandwidth efficiency (3 bit/s/Hz) than the turbo-coded system (1/3 bit/s/Hz). The tradeoff is the higher SNR required for BICM to achieve the PER threshold 2×10^{-3}. Moreover, turbo code is known to be very energy efficient with near-capacity performance. This is why we observe a huge difference of 12 dB between the values of b of the two systems.

For performance comparison, we consider the two different transmitting beam patterns shown in Figs. 6 and 7. These beam patterns are generated by end-fire antenna arrays with different numbers of antenna elements [15]. Beam pattern 1 is generated by six antenna elements, whereas beam pattern 2 is generated by ten antenna elements. The element separation is $\lambda/8$, where λ is the wavelength and is equal to 0.15 (m), assuming that the operating frequency of the wireless network is 2 GHz. The main lobe of beam pattern 1 (AIF of 0.6569 at $\eta = 4$ and 0.5699 at $\eta = 2.7$) is wider than that of beam pattern 2 (AIF of 0.5511 at $\eta = 4$ and 0.4545 at $\eta = 2.7$). Unless mentioned otherwise, the receiving antennas of the numerical examples presented in this paper are all omnidirectional (AIF of 1.0). The variance of shadowing is $\sigma = 6$ dB. In all of the numerical examples in this section, $r_0 = 0.1$ (in kilometers), and $K = 1$. We consider two different path loss exponents in our experiments: $\eta = 4$ for an obstructed environment in a building and $\eta = 2.7$ for an urban area [13].

In Figs. 8 and 9, the outage probability is shown for a turbo-coded system and a BICM system with $\lambda_M = 20.0$ and $\eta = 4$ under different values of p. From the figures, we see that beam pattern 2 has lower outage probability than beam pattern 1, and the omnidirectional antenna has the worst performance at all values of the load p. The interference power is indeed

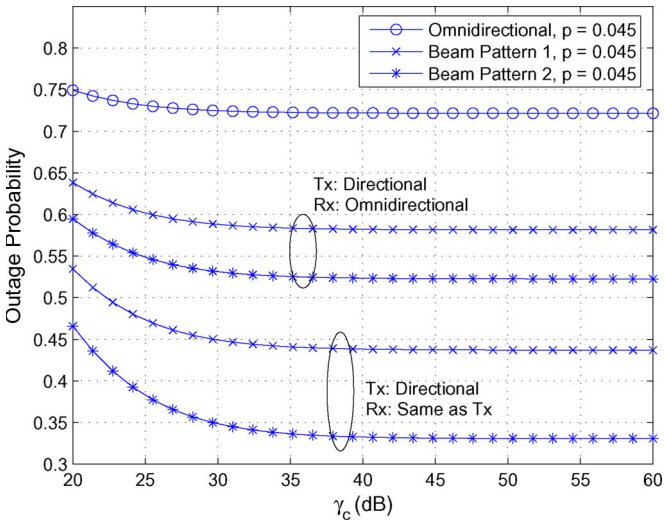

Fig. 10. Outage probability versus average received SNR γ_c with (1, 5/7) convolutional-coded 64-QAM in an urban area, Tx is directional, Rx is omnidirectional/directional, $\lambda_M = 20.0$ node/km^2, $b = 13.5$ dB, $\sigma = 6$ dB, $\eta = 2.7$, and $r_0 = 0.1$ km.

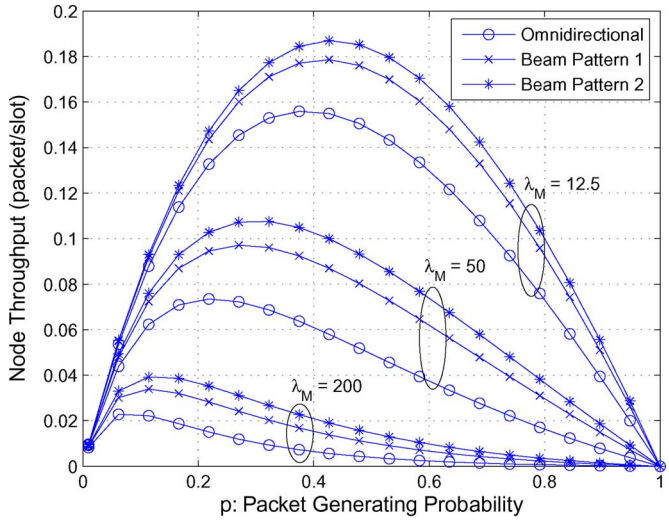

Fig. 11. Node throughput versus packet-generating probability p with (1, 33/37, 33/37) turbo code in an obstructed environment, $\gamma_c = 25$ dB, $\lambda_M = 12.5, 50.0, 200.0$ node/km^2, $b = 1.6$ dB, $\sigma = 6$ dB, $\eta = 4$, and $r_0 = 0.1$ km.

reduced by the narrower main lobe (smaller AIF), and thus, the outage probability is also reduced. We also observe that the outage probability has a nonzero floor as the average received signal SNR γ_c increases beyond 35 dB. When γ_c is large, it indicates that the noise power is small, compared to the signal and the interference power. Hence, the dominating factor of the performance degradation now is the interference from other nodes. Therefore, even if we increase the transmission power of all nodes by the same factor, the SINR remains almost the same, and so does the outage probability. In addition, note that, as p increases, i.e., the nodes generate packets with higher load, the outage probability also increases since there is more interference in the network. It is also observed that the turbo-coded system has much lower outage probability than the BICM system.

To compare the system performance in different wireless environments, we consider the BICM system in an urban area with a smaller path loss exponent $\eta = 2.7$. The outage probability versus the average received SNR γ_c is plotted in Fig. 10. If we compare Figs. 9 and 10, we can see that the performance in the urban area is worse than that in the obstructed environment at all SNRs. This is because path loss is much smaller in the urban area, and thus, the interference power from other nodes is less attenuated than that in the case of the obstructed area. To reject the interference, directional antenna should be applied to Rx for the receiving signal. In Fig. 10, we also plot the outage probability when Tx and Rx both use the same beam pattern for the transmitting and receiving signals. We can see that the outage probability is significantly reduced. This shows the great performance of directional antennas in rejecting interferences.

Finally, in Fig. 11, we plot the node throughput versus the packet-generating probability p for networks of different densities. The node throughput is defined as $p(1-p)(1-\phi_{r_0}(b))$, which denotes the average number of successfully transmitted/received packets per time slot. Note that factor $(1-p)$ comes from the fact that the nodes in an ALOHA ad hoc network are not allowed to be in transmitting and receiving modes at the same time. It is observed that the node throughput increases when directional antennas are used, and the throughput gain of using directional antennas grows as the network becomes more dense.

IV. Effect of Direction Estimation Error

In the previous analysis, Tx is assumed to know the direction to Rx, and thus, they are always perfectly aligned. This is not an easy task to achieve in reality. While it is not in the scope of this paper, two possible solutions are proposed here. One is to have each node include the antenna direction information, along with the node identification in the header of all transmitted packets. When a neighboring node B parses the packet header from node A and finds that node A is pointing the transmitting antenna to southwest, node B realizes right away that node A is in the direction of northeast. The information is then stored at node B, so it knows which direction to point at when transmitting to node A in the future. Another possible solution is to have all nodes equipped with Global Positioning System. The location information, along with the identification of each node, is included in the headers of all the packets it transmits. The neighboring node B can then keep track of the direction to node A by parsing the packet headers from node A. In a network of low traffic load, where nodes seldom transmit packets, the direction estimation accuracy can be enhanced by designing a protocol so that each node announces its location to its neighbors by periodically sending out broadcasting packets. In any of the solutions previously mentioned, it is always possible to have a direction estimation error at the neighboring nodes if node A moves between the instances of its packet transmissions (with direction/location information included in the headers). The existence of the direction estimation error has an impact on the outage probability. In general, the larger the beam width of a Tx beam pattern, the less sensitive the outage probability to the direction estimation error. However, less performance improvement will be achievable by the directional antenna. To

fully explore the tradeoff, it is desirable to analyze the outage probability, given the existence of the direction estimation error.

A. Modified Outage Probability

In practice, there are many factors that can affect the accuracy of the direction estimation, e.g., the estimation algorithm used, channel status, noise, interference, and MAC protocol. It is very difficult to characterize the direction estimation error in a deterministic way. Hence, we model it as a random variable δ_t with some given pdf $f_t(\delta_t)$. We define $\phi_{r_0}(b \mid \delta_t)$ as the outage probability, given an error of δ_t. From our previous analysis, we can derive the expression of $\phi_{r_0}(b \mid \delta_t)$ as

$$\phi_{r_0}(b \mid \delta_t) = 1 - \frac{1}{\sqrt{2\pi}\sigma\rho} \int_{-\infty}^{\infty} \exp\left\{ -\Lambda(b,x) r_0^2 \mathcal{A}_t(\delta_t) - \frac{b e^{-x} g_T(\theta_0)}{\gamma_c g_T(\theta_0 + \delta_t)} - \frac{x^2}{2\sigma^2\rho^2} \right\} dx \quad (22)$$

where

$$\mathcal{A}_t(\delta_t) \triangleq \frac{1}{2\pi} \int_0^{2\pi} \left(\frac{g_T(\theta)}{g_T(\theta_0 + \delta_t)} \right)^{\frac{2}{\eta}} d\theta \quad (23)$$

denotes the AIF of the Tx beam pattern $g_T(\theta)$, given an error of δ_t. By taking the expectation of $\phi_{r_0}(b \mid \delta_t)$ with respect to $f_t(\delta_t)$, we can obtain the outage probability

$$\phi_{r_0}(b) = 1 - \frac{1}{\sqrt{2\pi}\sigma\rho} \int_0^{2\pi} f_t(\delta_t) d\delta_t \int_{-\infty}^{\infty} \exp\left\{ -\Lambda(b,x) r_0^2 \times \mathcal{A}_t(\delta_t) - \frac{b e^{-x} g_T(\theta_0)}{\gamma_c g_T(\theta_0 + \delta_t)} - \frac{x^2}{2\sigma^2\rho^2} \right\} dx. \quad (24)$$

If Rx also has the ability of beam forming, then direction estimation error δ_r at Rx also needs to be taken into account. Given the pdf of δ_r, $f_r(\delta_r)$, we can obtain the outage probability after some manipulation, i.e.,

$$\phi_{r_0}(b) = 1 - \frac{1}{\sqrt{2\pi}\sigma\rho} \int_0^{2\pi} f_t(\delta_t) d\delta_t \int_0^{2\pi} f_r(\delta_r) d\delta_r \times \int_{-\infty}^{\infty} \exp\left\{ -\Lambda(b,x) r_0^2 \mathcal{A}_t(\delta_t) \mathcal{A}_r(\delta_r) - \frac{x^2}{2\sigma^2\rho^2} - \frac{b e^{-x} g_T(\theta_0) g_R(\theta_0)}{\gamma_c g_T(\theta_0 + \delta_t) g_R(\theta_0 + \delta_r)} \right\} dx \quad (25)$$

where

$$\mathcal{A}_r(\delta_r) \triangleq \frac{1}{2\pi} \int_0^{2\pi} \left(\frac{g_R(\theta)}{g_R(\theta_0 + \delta_r)} \right)^{\frac{2}{\eta}} d\theta \quad (26)$$

denotes the AIF of the Rx beam pattern $g_r(\theta)$, given an error of δ_r.

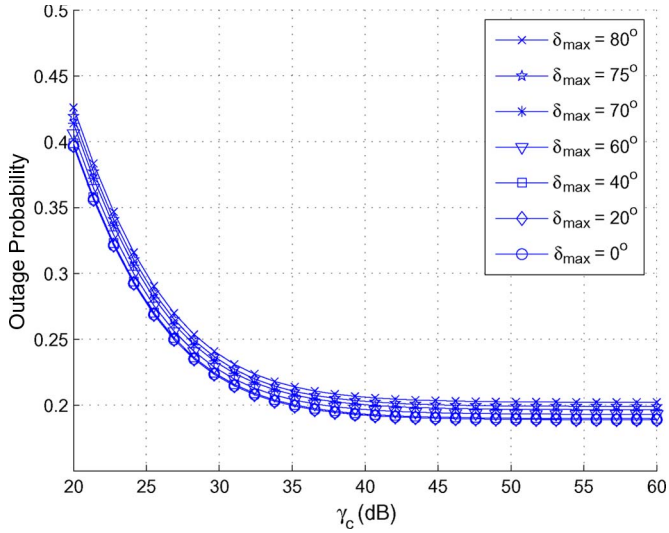

Fig. 12. Outage probability versus average received SNR γ_c with direction estimation error using beam pattern 1 (AIF = 0.6569) and (1, 5/7) convolutional-coded 64-QAM in an obstructed environment, λ_M = 20.0 node/km^2, b = 13.5 dB, σ = 6 dB, $\eta = 4$, $p = 0.045$, and $r_0 = 0.1$ km.

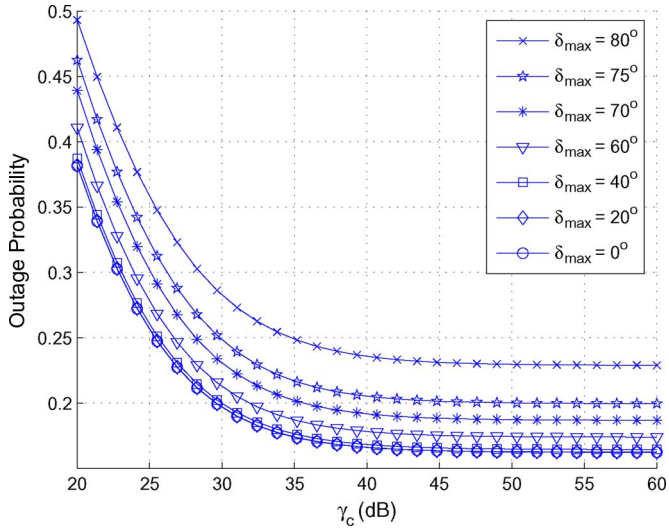

Fig. 13. Outage probability versus average received SNR γ_c with direction estimation error using beam pattern 2 (AIF = 0.5511) and (1, 5/7) convolutional-coded 64-QAM in an obstructed environment, λ_M = 20.0 node/km^2, b = 13.5 dB, σ = 6 dB, $\eta = 4$, $p = 0.045$, and $r_0 = 0.1$ km.

B. Numerical Examples

Assume that only Tx has beam-forming ability and that the direction estimation error δ_t is uniformly distributed in the interval $[-\delta_{\max}, \delta_{\max}]$, as in the case in the MAC protocols for IEEE 802.11 with directional antennas [1], [2], which has a fixed number of beam directions B. The maximum error $\delta_{\max}$ is then $180^\circ/B$.

In Figs. 12 and 13, we show the outage probability of the two beam patterns (defined in Section III-C) in an obstructed environment for various values of $\delta_{\max}$. We see that beam pattern 1 is less sensitive to direction estimation error since it has a wider main lobe than beam pattern 2. From Fig. 7, we see that the main lobe width of beam pattern 2 is roughly 120°. When $\delta_{\max}$ is larger than 60°, it is possible for Rx to be totally off from the coverage of the main lobe, which severely degrades

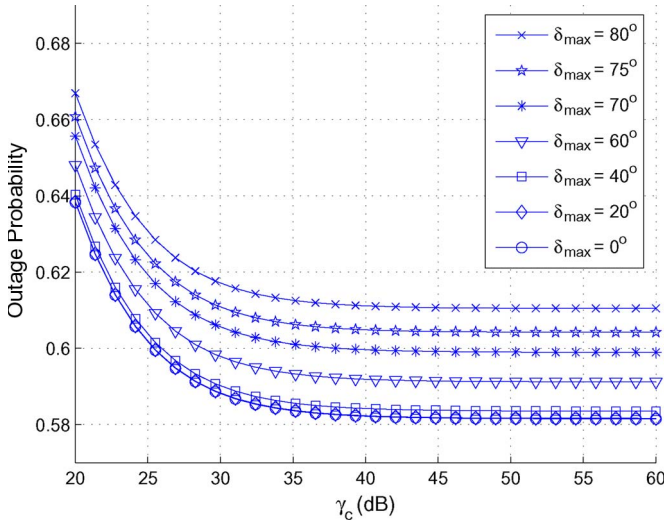

Fig. 14. Outage probability versus average received SNR γ_c with direction estimation error using beam pattern 1 (AIF $= 0.5699$) and (1, 5/7) convolutional-coded 64-QAM in an urban area, $\lambda_M = 20.0$ node/km^2, $b = 13.5$ dB, $\sigma = 6$ dB, $\eta = 2.7$, $p = 0.045$, and $r_0 = 0.1$ km.

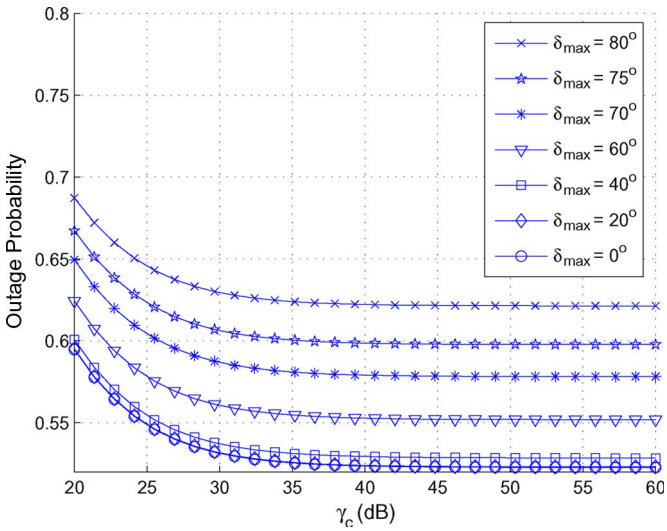

Fig. 15. Outage probability versus average received SNR γ_c with direction estimation error using beam pattern 2 (AIF $= 0.4545$) and (1, 5/7) convolutional-coded 64-QAM in an urban area, $\lambda_M = 20.0$ node/km^2, $b = 13.5$ dB, $\sigma = 6$ dB, $\eta = 2.7$, $p = 0.045$, and $r_0 = 0.1$ km.

system performance. This is why the outage probability of beam pattern 2 starts to abruptly increase after $\delta_{\max}$ exceeds one half of the main beam width (60°) by some amount of tolerance (15°). From the figure, we can conclude that, for the MAC protocols in [1] and [2], beam pattern 2 still works fine if the number of beam directions B is greater than 3, but the performance starts to severely degrade when B goes below 3.

In Figs. 14 and 15, we show the outage probability of the two beam patterns in an urban area. Since the interference power is less attenuated in the urban area, any direction estimation error can severely attenuate the SINR. As a result, we can see that the outage probability is more sensitive to the direction estimation error for both beam patterns. However, still, the wider beam pattern 1 is less sensitive to the direction estimation error than beam pattern 2. We also observe from Fig. 15 that the outage probability starts to abruptly increase right before $\delta_{\max}$

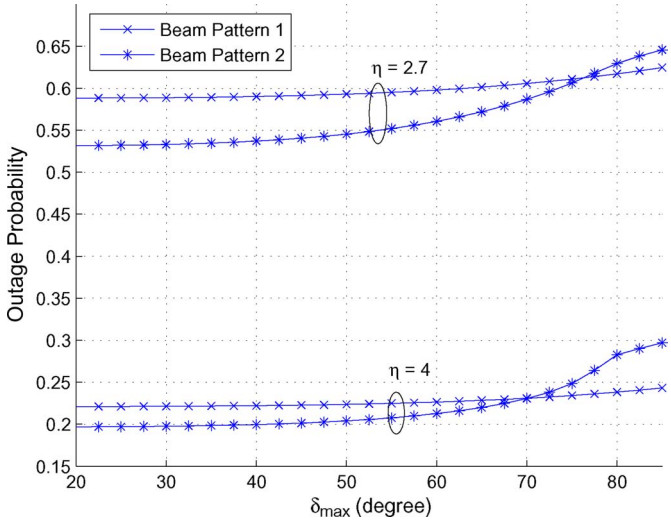

Fig. 16. Outage probability versus $\delta_{\max}$ using (1, 5/7) convolutional-coded 64-QAM, $\gamma_c = 30$ dB, $\lambda_M = 20.0$ node/km^2, $b = 13.5$ dB, $\sigma = 6$ dB, $p = 0.045$, and $r_0 = 0.1$ km.

reaches one half of the main lobe width of beam pattern 2. The previous tolerance of 15° no longer exists, because the system performance is extremely sensitive to the direction estimation error in the urban area.

In Fig. 16, we plot the outage probability versus $\delta_{\max}$ using both beam patterns, with γ_c fixed at 30 dB. We see that the outage probability curves of beam patterns 1 and 2 intersect in the figure. At small $\delta_{\max}$, beam pattern 2 performs better because of its smaller beam width. However, once $\delta_{\max}$ exceeds one half of the beam width of beam pattern 2, the outage probability begins to rapidly increase. On the other hand, beam pattern 1 is not that sensitive to $\delta_{\max}$ due to its wider beam width. As a result, beam pattern 1 outperforms beam pattern 2 at a large $\delta_{\max}$. Through our analysis, one can determine the beam pattern to use, given that the accuracy of the direction estimation $\delta_{\max}$ is known.

V. Analysis of Network Throughput and Transport Capacity

Network throughput and transport capacity are commonly used to measure the performance of wireless networks. Both are analyzed in this section for wireless networks with directional antennas. To find the best possible network performance, the direction estimation error is assumed to be 0 in the following analysis. However, the result can easily be generalized to take into account the direction estimation error.

A. Network Throughput

The network throughput of a wireless network is defined as the average number of successfully transmitted information bits per unit area per second per hertz, which can be approximated by

$$S(b) \approx \lambda_M p(1-p) R \int_0^{r_{\max}} f(r_0)\left(1-\phi_{r_0}(b)\right) dr_0 \times \left(\frac{\text{bit}}{\text{unit area} \cdot \text{sec} \cdot \text{Hz}}\right) \quad (27)$$

where $\lambda_M p$ accounts for the average number of simultaneous transmissions per unit area (1/unit area), $(1-p)$ is the probability for each receiving node to be in receiving mode, R is the rate of the coded modulation used (in bits per second per hertz), and the integral $\int_0^{r_{\max}} f(r_0)(1-\phi_{r_0}(b))dr_0$ is the probability of successful transmission. Equation (27) is said to be an approximation since it assumes that the successful transmissions of different nodes are independent events, which is not true in reality since transmitting nodes interfere with each other. Recall that $f(r_0)$ denotes the pdf of distance r_0 between Tx and Rx, which is determined by the MAC protocol and the network protocol. Since the values of r_0 of different Tx–Rx pairs in a network are not necessarily the same, we need to take the expectation of $\phi_{r_0}(b)$ with respect to r_0 when computing system throughput.

The system throughput of a wireless network is affected by the node density of the network. When the density is high, the interference problem becomes more serious, and thus, the outage probability increases. This will affect the system throughput in (27). On the other hand, the outage probability is smaller if the density is low, but, since not many nodes are transmitting, this might cause the network resources (bandwidth) to be wasted without producing much system throughput. Our outage probability analysis can be used to find the optimal node density for a wireless network. We consider two different $f(r_0)$'s. The first case is that the network is controlled where all Tx–Rx pairs in the network have the same distance between the two nodes (similar to the case of mesh network). Hence, $f(r_0)=\delta(r_0-c)$, where c is a constant. From (27), the system throughput is approximately

$$S_1(b) \approx \lambda_M p(1-p)\left(1-\phi_c(b)\right) R \tag{28}$$

where $\phi_c(b)$ can be computed through (21).

On the other hand, if the network allows a node to transmit signals to any node within a distance of $r_{\max}$, then $f(r_0)=2r_0/r_{\max}^2$. Substitute $\phi_{r_0}(b)$ in (27) by (21). After some manipulations, we can obtain the system throughput approximation as

$$S_2(b) \approx \frac{\lambda_M p(1-p)R}{\sqrt{2\pi}\sigma\rho r_{\max}^2} \int_{-\infty}^{\infty} \frac{1-\exp\left\{-\Lambda(b,x) r_{\max}^2 \mathcal{A}_t \mathcal{A}_r\right\}}{\Lambda(b,x)\mathcal{A}_t\mathcal{A}_r} \times \exp\left\{-\frac{be^{-x}}{\gamma_c} - \frac{x^2}{2\sigma^2\rho^2}\right\} dx. \tag{29}$$

Consider the same setup as in Section III-C. The rate of BICM is $R=3$ (in bits per second per hertz), and that of the turbo code is $R=1/3$ (in bits per second per hertz). We first consider system throughput $S_1(b)$ for the case where the distance between Tx and Rx is fixed at $r_0=0.1$ km for all Tx–Rx pairs. The system throughput approximation $S_1(b)$ versus λ_M in an obstructed environment ($\eta=4$) is plotted in Fig. 17. It is observed that the system throughput of BICM is higher than the turbo-coded system at small λ_M. This is because the interference problem is not large at small λ_M, and thus, BICM can maintain a relatively small outage probability. Under such circumstances, the higher bandwidth efficiency of BICM, compared to that of the turbo-coded system, results in the larger system throughput of BICM. However, when λ_M becomes large, the interference problem causes BICM to have a very large outage probability; it is so large that even the high bandwidth efficiency of BICM cannot make up for the loss of the system throughput. As a result, the turbo-coded system starts to have a higher system throughput than BICM. In any case, we can see that there exists an optimal node density for each setup. Beam pattern 2 of the smallest AIF again has the best performance in all cases, and the turbo-coded system has higher optimal node density than BICM.

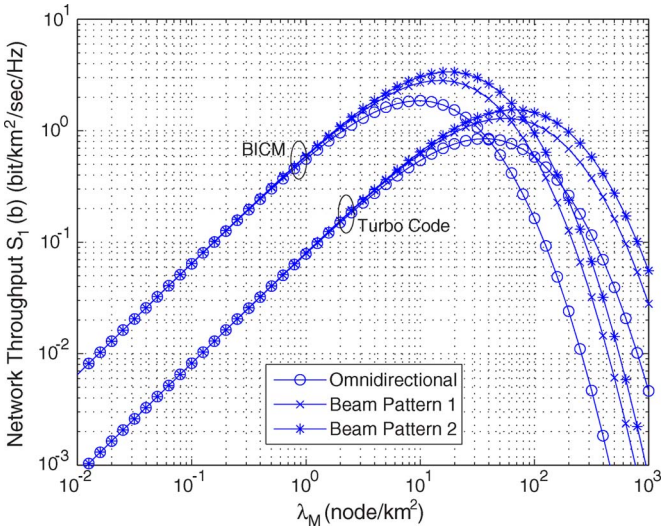

Fig. 17. System throughput $S_1(b)$ versus node density λ_M with $r_0=c=0.1$ km in an obstructed environment, $\gamma_c=25$ dB, $\sigma=6$ dB, $\eta=4$, and $p=0.5$.

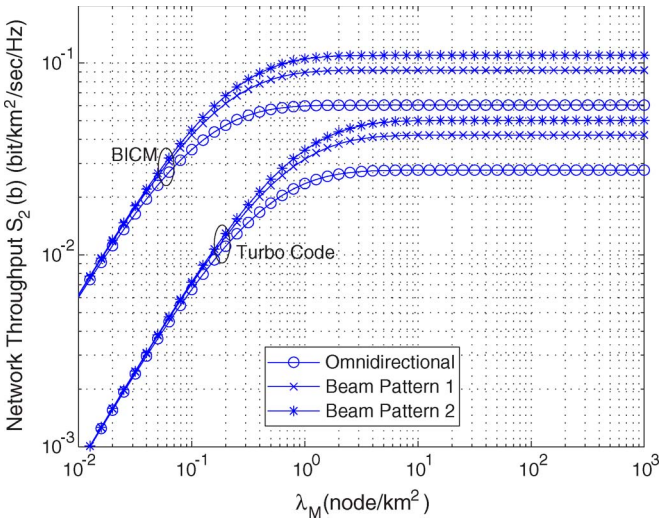

Fig. 18. System throughput $S_2(b)$ versus node density λ_M with $r_{\max}=1$ km in an obstructed environment, $\gamma_c=25$ dB, $\sigma=6$ dB, $\eta=4$, and $p=0.5$.

In Fig. 18, we plot the system throughput approximation $S_2(b)$ versus λ_M, where r_0 is no longer fixed, and $r_{\max}=1$ km. It is observed that the system throughput converges as λ_M increases. The asymptotic system throughput when λ_M and γ_c are both large can be derived as

$$\lim_{\substack{\gamma_c\to\infty \\ \lambda_M\to\infty}} S_2(b) \approx \frac{(1-p)R}{r_{\max}^2 \frac{2\pi^2}{\eta}\csc\left(\frac{2\pi}{\eta}\right) b^{\frac{2}{\eta}} \mathcal{A}_t\mathcal{A}_r}. \tag{30}$$

B. Transport Capacity

The transport capacity of a network characterizes the capability of the network to transport information toward the destination [12]. It can also be regarded as the accumulated sum of the link progress of the links that has taken place in a network area, where the link progress is defined as the product of the hop distance and the local throughput of the link between a Tx–Rx node pair [5], [6]. The network transport capacity can be expressed as

$$T(b) \approx \lambda_M p(1-p) R \int_0^{r_{\max}} f(r_0) r_0 \left(1 - \phi_{r_0}(b)\right) dr_0 \times \left(\frac{\text{bit} \cdot \text{unit distance}}{\text{unit area} \cdot \text{sec} \cdot \text{Hz}}\right). \quad (31)$$

Compared to (27), it is easy to see that the major difference that distinguishes the transport capacity from the throughput is the weighting of the hop distance r_0 in the integral. It was mentioned by Gupta and Kumar [12] that, to achieve a high transport capacity, a node should communicate only with nearby nodes within a distance of order $\Theta(1/\sqrt{\lambda_M})$. In our notations, this translates to $r_{\max} = \Theta(1/\sqrt{\lambda_M})$. If we simply let $r_{\max} = \lambda_M^{-1/2}$, we have $f(r_0) = 2r_0/r_{\max}^2 = 2\lambda_M r_0$. Then, from (21) and (31), we have

$$\begin{aligned} T(b) &\approx \frac{\lambda_M p(1-p) R}{\sqrt{2\pi}\sigma\rho} \int_0^{\lambda_M^{\frac{-1}{2}}} 2\lambda_M r_0^2 dr_0 \\ &\quad \times \int_{-\infty}^{\infty} e^{-\Lambda(b,x) r_0^2 \mathcal{A}_t \mathcal{A}_r - \frac{be^{-x}}{\gamma_c} - \frac{x^2}{2\sigma^2\rho^2}} dx \\ &= \frac{2\lambda_M^2 p(1-p) R}{\sqrt{2\pi}\sigma\rho} \int_{-\infty}^{\infty} e^{-\frac{be^{-x}}{\gamma_c} - \frac{x^2}{2\sigma^2\rho^2}} dx \\ &\quad \times \int_0^{\lambda_M^{\frac{-1}{2}}} r_0^2 e^{-\Lambda(b,x)\mathcal{A}_t\mathcal{A}_r r_0^2} dr_0 \\ &= \frac{\sqrt{2}\lambda_M^2 p(1-p) R}{\sqrt{\pi}\sigma\rho} \int_{-\infty}^{\infty} e^{-\frac{be^{-x}}{\gamma_c} - \frac{x^2}{2\sigma^2\rho^2}} dx \\ &\quad \times \int_0^{\lambda_M^{-\frac{1}{2}}} r_0^{3-1} \left[\lambda_M^{-\frac{1}{2}} - r_0\right]^{1-1} e^{-\Lambda(b,x)\mathcal{A}_t\mathcal{A}_r r_0^2} dr_0. \end{aligned} \quad (32)$$

Now, apply the integration formula [16]

$$\begin{aligned} &\int_0^u x^{\nu-1}[u-x]^{\mu-1} e^{\beta x^n} dx \\ &\quad = B(\mu,\nu) u^{\mu+\nu-1} \\ &\qquad \times {}_nF_n\left(\frac{\nu}{n}, \ldots, \frac{\nu+n-1}{n}; \frac{\mu+\nu}{n}, \ldots, \frac{\mu+\nu+n-1}{n}; \beta u^n\right) \end{aligned} \quad (33)$$

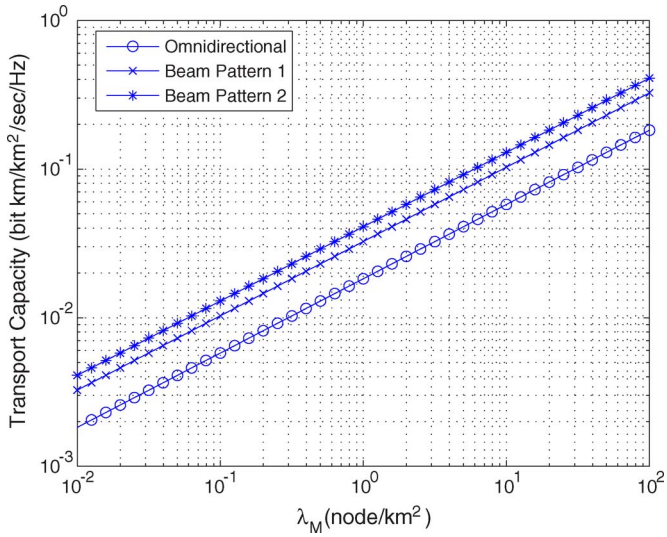

Fig. 19. Transport capacity versus node density λ_M using (1, 5/7) convolutional-coded 64-QAM in an obstructed environment with $r_{\max} = \lambda_M^{-1/2}$ km, $\gamma_c = 25$ dB, $b = 13.5$ dB, $\sigma = 6$ dB, and $\eta = 4$, $p = 0.5$.

to the inner integral of (32), where $B(\cdot,\cdot)$ denotes the beta function, and ${}_nF_n(\cdots;\cdots;\cdot)$ denotes the generalized hypergeometric series. We thus have

$$\begin{aligned} T(b) &\approx \frac{\sqrt{2}\lambda_M^2 p(1-p) R}{\sqrt{\pi}\sigma\rho} \int_{-\infty}^{\infty} e^{-\frac{be^{-x}}{\gamma_c} - \frac{x^2}{2\sigma^2\rho^2}} B(1,3) \lambda_M^{-\frac{3}{2}} \\ &\quad \times {}_2F_2\left(\frac{3}{2}, 2; 2, \frac{5}{2}; -\Lambda(b,x)\mathcal{A}_t\mathcal{A}_r {\lambda_M}^{-\frac{2}{2}}\right) dx \\ &= \frac{\sqrt{2\lambda_M} p(1-p) R}{\sqrt{\pi}\sigma\rho} \int_{-\infty}^{\infty} e^{-\frac{be^{-x}}{\gamma_c} - \frac{x^2}{2\sigma^2\rho^2}} B(1,3) \\ &\quad \times {}_2F_2\left(\frac{3}{2}, 2; 2, \frac{5}{2}; -\pi p e^{\frac{2\sigma^2\rho^2}{\eta^2}} \frac{2\pi}{\eta} \csc\left(\frac{2\pi}{\eta}\right) \right. \\ &\qquad \left. \times b^{\frac{2}{\eta}} e^{\frac{-2x}{\eta}} \mathcal{A}_t\mathcal{A}_r\right) dx. \end{aligned} \quad (34)$$

Note that the last line comes from substituting (18) into the first line of (34). We can observe that there exists no λ_M in the integral of (34). Therefore, the transport capacity of the network is of the same order as $\sqrt{\lambda_M}$. This matches the well-known network transport capacity $\Theta(\sqrt{\lambda_M})$ derived by Gupta and Kumar in [12]. In Fig. 19, we plot network transport capacity $T(b)$ versus node density λ_M computed from (31). It can be seen that $T(b)$ is indeed of the same order as $\sqrt{\lambda_M}$. In addition, it is obvious from the figure that the beam pattern with smaller AIF always has a higher transport capacity.

VI. Conclusion

In this paper, the performance of wireless networks with directional antennas of arbitrary beam pattern has been analyzed. By combining with the performance analysis of BICM and turbo codes, we have analyzed the performance of wireless networks with directional antennas for each coding/modulation scheme used. The characteristic value that determines the

performance of a beam pattern has been found, which is useful for the performance comparison of different beam patterns in random networks. The effect of direction estimation error on the network performance has also been analyzed. Finally, our analysis has been applied to find the throughput and the transport capacity of the wireless networks. Results show that significant gains on network throughput and transport capacity can be achieved by directional antennas. Although the analysis shown in this paper focuses on 2-D beam patterns, the analysis can easily be extended to 3-D case, which is useful if nodes are distributed over a wide range of altitudes. The performance analysis in this paper provides system designers a way to characterize the system performance under different combinations of beam patterns and coding/modulation schemes, as long as the performance can be expressed in terms of outage probability (for instance, the throughput). This is useful for designers to optimize network performance. Future work on this analysis includes the design of automatic repeat request (ARQ), power control algorithm, and adaptive physical layer (PHY) for wireless networks with directional antennas.

REFERENCES

[1] A. Nasipuri, K. Li, and U. R. Sappidi, "Power consumption and throughput in mobile ad hoc networks using directional antennas," in *Proc. Int. Conf. Comput. Commun. Netw.*, Oct. 2002, pp. 620–626.

[2] T. Korakis, G. Jakllari, and L. Tassiulas, "A MAC protocol for full exploitation of directional antennas in ad-hoc wireless networks," in *Proc. ACM MobiHoc*, Jun. 2003, pp. 98–107.

[3] *IEEE Standard for Local and Metropolitan Area Networks—Part 16: Air Interface for Fixed and Mobile Broadband Wireless Access Systems Amendment 2: Physical and Medium Access Control Layers for Combined Fixed and Mobile Operation in Licensed Bands and Corrigendum 1*, IEEE Std. 802.16, 2006.

[4] *WPAN Millimeter Wave Alternative PHY Task Group 3c (TG3c)*, IEEE Std. 802.15, 2008.

[5] M. Zorzi and S. Pupolin, "Outage probability in multiple access packet radio networks in the presence of fading," *IEEE Trans. Veh. Technol.*, vol. 43, no. 3, pp. 604–610, Aug. 1994.

[6] M. Zorzi and R. Rao, "Capture and retransmission control in mobile radio," *IEEE J. Sel. Areas Commun.*, vol. 12, no. 8, pp. 1289–1298, Oct. 1994.

[7] W. Fung, M. Hamdi, and R. Murch, "Performance evaluation of mobile radio slotted ALOHA with smart antennas," in *Proc. IEEE Wireless Commun. Netw. Conf.*, 1999, vol. 1, pp. 271–275.

[8] M. Kang, M. Alouini, and L. Yang, "Outage probability and spectrum efficiency of cellular mobile radio systems with smart antennas," *IEEE Trans. Commun.*, vol. 50, no. 12, pp. 1871–1877, Dec. 2002.

[9] D. Bertsekas and R. Gallager, *Data Networks*, 2nd ed. Englewood Cliffs, NJ: Prentice-Hall, 1992.

[10] P. Yeh, S. Zummo, and W. Stark, "Error probability of bit-interleaved coded modulation (BICM) in wireless environments," *IEEE Trans. Veh. Technol.*, vol. 55, no. 2, pp. 722–728, Mar. 2006.

[11] P. Yeh, A. Yilmaz, and W. Stark, "On the error floor analysis of turbo codes: Weight spectrum estimation (WSE) scheme," in *Proc. IEEE Int. Symp. Inf. Theory*, Jul. 2003, p. 439.

[12] P. Gupta and P. R. Kumar, "The capacity of wireless networks," *IEEE Trans. Inf. Theory*, vol. 46, no. 2, pp. 388–404, Mar. 2000.

[13] T. S. Rappaport, *Wireless Communications*, 2nd ed. Upper Saddle River, NJ: Prentice-Hall, 1996.

[14] J. G. Proakis, *Digital Communications*, 4th ed. New York: McGraw-Hill, 2000.

[15] C. A. Balanis, *Antenna Theory*, 2nd ed. New York: Wiley, 1997.

[16] I. S. Gradshteyn and I. M. Ryshik, *Table of Integrals, Series, and Products*, 6th ed. San Diego, CA: Academic, 2000.

Ping-Cheng Yeh (M'05) received the B.S. degree in mathematics and the M.S. degree in electrical engineering from National Taiwan University, Taipei, Taiwan, R.O.C., in 1996 and 1998, respectively, and the Ph.D. degree in electrical engineering and computer science from the University of Michigan, Ann Arbor, in 2005.

He is currently an Assistant Professor with the Department of Electrical Engineering and the Graduate Institute of Communication Engineering, National Taiwan University. His research interests include channel coding, coded modulation, directional antennas, and cross-layer design in wireless networks.

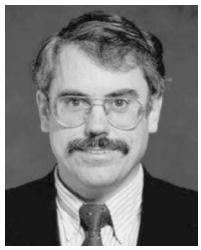

Wayne E. Stark (S'77–M'78–SM'94–F'98) received the B.S. (with highest honors), M.S., and Ph.D. degrees in electrical engineering from the University of Illinois, Urbana, in 1978, 1979, and 1982, respectively.

Since September 1982, he has been a Faculty Member with the Department of Electrical Engineering and Computer Science, University of Michigan, Ann Arbor, where he is currently a Professor. He was selected by the National Science Foundation as a 1985 Presidential Young Investigator and was also the Principal Investigator of an Army Research Office Multidisciplinary University Research Initiative (MURI) project on Low Energy Mobile Communications. His research interests are coding and communication theory, particularly for spread-spectrum and wireless communication networks.

Dr. Stark is a member of Eta Kappa Nu, Phi Kappa Phi, and Tau Beta Pi. From 1984 to 1989, he was an Editor for Communication Theory for the IEEE TRANSACTIONS ON COMMUNICATION in the area of spread-spectrum communications. He was also involved in the planning and organization of the 1986 International Symposium on Information Theory, which was held in Ann Arbor. He was the recipient of the IEEE Military Communications Conference Technical Achievement Award in 2002.

Salam A. Zummo (M'00) received the B.Sc. and M.Sc. degrees (with highest honors) in electrical engineering from King Fahd University of Petroleum and Minerals (KFUPM), Dhahran, Saudi Arabia, in 1998 and 1999, respectively, and the Ph.D. degree from the University of Michigan, Ann Arbor, in 2003.

He is currently with the Department of Electrical Engineering, KFUPM. His research interests include error control coding, coded modulation, adaptive modulation, MIMO, multiuser diversity, user cooperation, iterative receivers, interference modeling and analysis, and cross-layer design of wireless communication networks.